Switchable Assembly and Guidance of Colloidal Particles on an All-Dielectric One-Dimensional Photonic Crystal

Fengya Lu,[1] Yan Kuai,[1] Junxue Chen,[2] Xi Tang,[1] Yifeng Xiang,[1] Yang Liu,[1] Pei Wang,[1] Joseph. R. Lakowicz,[3] and Douguo Zhang[1,*]

[1] *Advanced Laser Technology Laboratory of Anhui Province and Institute of Photonics, Department of Optics and Optical Engineering, University of Science and Technology of China, Hefei, Anhui 230026, China*

[2] *School of Science, Southwest University of Science and Technology, Mianyang, Sichuan 621010, China*

[3] *Center for Fluorescence Spectroscopy, Department of Biochemistry and Molecular Biology, University of Maryland School of Medicine, 725 West Lombard St., Baltimore, Maryland 21201, USA*

(Received 5 November 2019; revised manuscript received 3 December 2019; published 13 January 2020)

Dielectric multilayer photonic-band-gap structures, called one-dimensional photonic crystals (1DPCs), have drawn considerable attention in the fields of physics, chemistry, and biophotonics. Here, experimental results verify the feasibility of a 1DPC working as a substrate for switchable manipulations of colloidal microparticles. The optically induced thermal convective force on a 1DPC can assemble colloidal particles that are dispersed in a water solution, while the photonic scattering force on the same 1DPC caused by propagating evanescent waves can guide these particles. Additionally, in the 1DPC, one internal mode can be excited that has seldom been noticed previously. This mode shows an ability to assemble particles over large areas even when the incident power is low. The assembly and guidance of colloidal particles on the 1DPC are switchable just through tuning the polarization and angle of the incident laser beam. Numerical simulations are carried out, which are consistent with these experimental observations.

DOI: 10.1103/PhysRevApplied.13.014020

I. INTRODUCTION

The broad appeal of optical tweezers has come about because of their noncontact nature, and microscopic objects can be picked up, delivered to a desired place in order to facilitate a measurement or a reaction, and then brought back to their initial position [1,2]. However, due to the limited magnitude of the optical trapping forces at high input power (usually up to 10^2–10^3 mW) [3–5], it is difficult to assemble or guide large numbers of small objects that are dispersed in liquids [6,7]. Within this limit, it has been found that evanescent waves at a dielectric or metal interface can manipulate particles over large areas at lower power. A colloidal particle placed in the vicinity of an evanescent wave will be guided in the direction of the evanescent wave vector by transfer of momentum from the propagating evanescent wave to the dielectric particle (the photonic scattering force) [8–16]. Besides the optical field, photothermal manipulation techniques provide versatile control of diverse species of colloidal particles; the strong temperature gradients of the optothermal field can cause optothermal-matter coupling phenomena through a combination of Marangoni convection, thermophoresis, thermoelectricity, and photophoresis [17–20]. Many methods for large-scale trapping of dielectric particles have been proposed, combining optical forces and optically induced thermal forces. Different competing forces dominate, leading to markedly different particle dynamics [21–24].

In the work presented here, manipulations of colloidal particles placed on a dielectric multilayer photonic-band-gap (PBG) structure are investigated experimentally and numerically. This structure is called a one-dimensional photonic crystal (1DPC), and has emerged as a unique structure for exciting Bloch surface waves (BSWs) [25] that can be used in imaging, sensing, two-dimensional optical elements, and other applications [26–32]. In fact, in addition to BSWs, evanescent waves can also be excited on the surface of this 1DPC through total internal reflection (TIR). Because of the existence of the PBG, these evanescent waves are sensitive to the polarization and angle of the incident laser beam, and thus will induce different forces on the colloidal particles; this has not been fully explored before [33,34]. Furthermore, for this 1DPC, one internal mode can be excited inside the multilayer structure and then the electromagnetic field will be localized inside the 1DPC. Under continuous illumination with a laser beam, heat will certainly be generated inside the 1DPC and then diffuse to the surface. The effect of this heat on the manipulation of colloidal particles has also not been carefully

*dgzhang@ustc.edu.cn

investigated before [35]. In the present work, manipulation of colloidal particles enabled by evanescent waves and the internal mode of the 1DPC is investigated experimentally and numerically, and shows different phenomena from the manipulation of colloidal particles using evanescent waves on a conventional glass/water interface [36].

II. RESULTS AND DISCUSSION

A. Configuration of the experimental setup and the 1DPC

Figure 1(a) shows a schematic diagram of the experimental setup, which is based on an inverted optical microscope. The center wavelength of the laser beam, which is used for the optical manipulations, is 640 nm. The polarization of the incident laser beam is controlled using a polarizer and a half-wave plate. Using a pair of scanning galvanometers and a focusing lens, the expanded and collimated incident laser beam can then be focused on any point in the back focal plane (BFP) of the objective [100×, numerical aperture (NA) 1.49] [32]. The expanded and collimated beam then exits the objective and strikes the substrate at a specific angle of incidence (θ). This angle θ is determined by the position of the focused point on the BFP, as illustrated in Fig. 1(a). The propagation direction of the incident beam relative to the normal plane of the multilayer structure can be defined using the two angles θ and Ψ illustrated in Fig. 1(a). Use of high-speed scanning galvanometers means that the angles of incidence θ and Ψ can be changed very quickly (in less than 1 ms). The laser beam reflected from the 1DPC is rejected by a band-pass filter, meaning that only the light from the white-light illuminator can reach the camera, and then the motions of the manipulated particles can be monitored clearly.

The dielectric multilayers are fabricated via plasma-enhanced chemical vapor deposition (PlasmaPro System 100, Oxford) of SiO_2 and Si_3N_4 on a standard microscope cover glass (12-548C, Fisher Scientific, 0.17 mm thickness) under a vacuum of less than 0.0133 Pa and at a temperature of 300 °C. The thicknesses of these layers are 66 nm (Si_3N_4) and 110 nm (SiO_2). There are 14 layers in total. The thickness of the top SiO_2 layer is approximately 200 nm, as shown in Fig. 1(b). The plane of incidence is the X-Z plane [Fig. 1(b)]. One drop of a water-based solution containing the colloidal particles is placed on the 1DPC. The mean diameter of these particles is approximately 2 μm. To check the response of the 1DPC to incident beams with different polarizations, an expanded white-light beam is used to fully fill the rear aperture of the objective and is then focused onto the 1DPC. The reflected light is collected using the same objective (100×, NA 1.49). The BFP of the objective is imaged using a scientific complementary metal-oxide-semiconductor (sCMOS) camera. A band-pass filter with a center wavelength of 640 nm is placed in front of the sCMOS camera to filter the reflected light. The captured BFP image of the light reflected from the 1DPC is shown in Fig. 1(c). The white line with the double arrowhead in Fig. 1(c) represents the incident

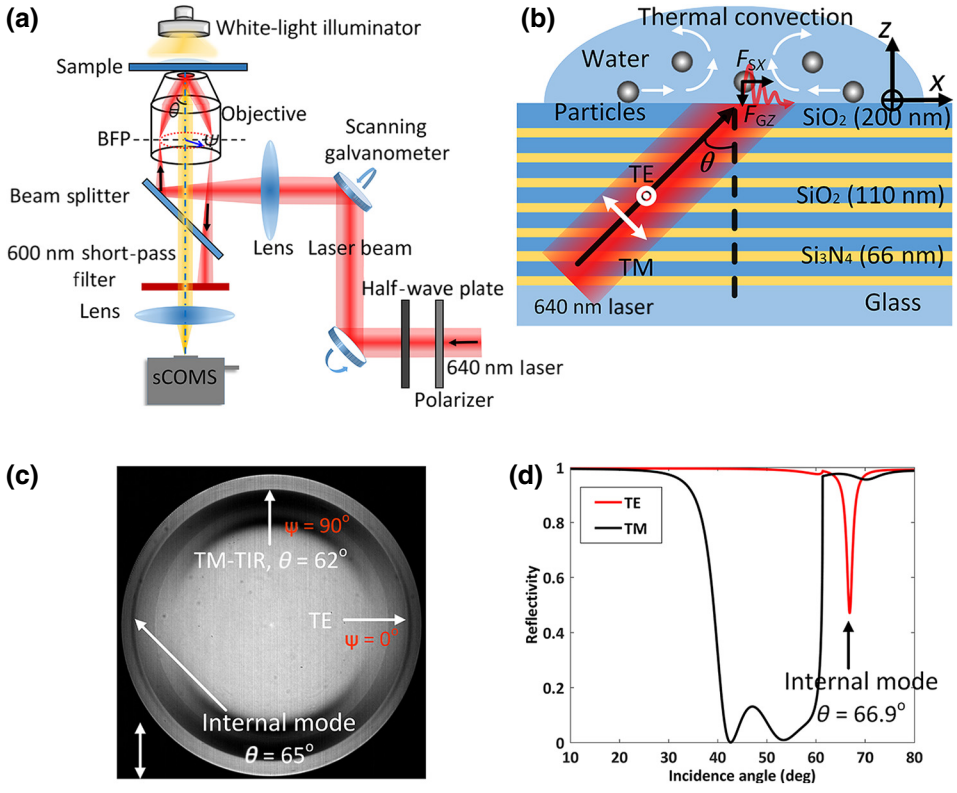

FIG. 1. Schematic illustration of the experimental setup, the 1DPC and its BFP image, and the calculated angle-dependent reflection curves. (a) Experimental setup. (b) Sample on (a), with the 1DPC acting as a substrate for the colloidal particles in a water-based solution. F_{SX} and F_{GZ} are the photonic scattering force and photonic gradient force, respectively. (c) BFP image of the 1DPC. The wavelength of the incident laser beam is 640 nm. (d) Calculated reflectance of the 1DPC versus angle of incidence under TE- and TM-polarized illumination.

polarization. The objective lens is axially symmetric with respect to the optical path, so, as illustrated in the BFP image, the incident light along the direction $\Psi = 0°$ has a transverse electric (TE) polarization, while that along the direction $\Psi = 90°$ has a transverse magnetic (TM) polarization, relative to the surface plane of the 1DPC. Based on the known NA of the objective, the TIR angle for the TM incident beam can be derived to be $\theta = 62°$, which is consistent with the results of a numerical calculation [arcsin(1.33/1.515)]. This BFP image clearly shows that the intensity of the reflected light for the TE-polarized incident beam differs from that for the TM-polarized incident beam, which indicates that the response of the 1DPC to the incident beam is polarization dependent. There is also a pair of dark arcs showing on the BFP image, which is a signature of the excitation of an internal mode. The excitation angle can be derived to be about $\theta = 65°$. Based on the known incident polarization, it can be deduced that this internal mode can only be excited using a TE-polarized beam [35]. The difference is illustrated more clearly in the incidence-angle-dependent reflectance curves shown in Fig. 1(d), which are calculated based on the transfer matrix method (TMM) [37]. According to the TMM, the expansion coefficients of the fields in the glass substrate and the water can be related via the matrix product

$$\begin{pmatrix} A_{\text{water}} \\ B_{\text{water}} \end{pmatrix} = \begin{pmatrix} m_{11} & m_{12} \\ m_{21} & m_{22} \end{pmatrix} \begin{pmatrix} A_{\text{glass}} \\ B_{\text{glass}} \end{pmatrix}, \tag{1}$$

where A_{glass} and B_{glass} are the amplitudes of the incident and reflected waves, respectively, in the glass substrate, and A_{water} and B_{water} are the amplitudes of the incident and reflected waves, respectively, in the water; m_{ij} (i, $j = 1, 2$) are the matrix elements of the transfer matrix. In the present work, the incident beam is incident on the dielectric multilayer from the glass substrate ($A_{\text{glass}} = 1$, $B_{\text{water}} = 0$). Then, the reflectance of the incident beam can be expressed as

$$R = \left| \frac{B_{\text{glass}}}{A_{\text{glass}}} \right|^2 = \left| -\frac{m_{21}}{m_{22}} \right|^2. \tag{2}$$

When the incident beam is TM polarized, there is a broad dip (indicating a low reflectivity) below the TIR angle (62°), which is consistent with the BFP image. In contrast, when the incident beam is TE polarized, no such broad dip appears below the TIR angle, but a narrow dip appears at 66.9° that corresponds to the internal-mode-excitation resonance. This calculated angle is nearly consistent with that measured using the BFP imaging technique [65°, Fig. 1(c)].

B. Experimental demonstrations of assembly and guidance of colloidal particles placed on 1DPC

First, the angle of incidence of the laser beam is set at about 63°, which is larger than the TIR angle, but lower than the angle for exciting the internal mode. The power of the incident laser beam is measured by placing the sensor of a power meter (microscope power sensor, S170C, Thorlab) in the front focal plane of the objective [replacing the sample, as shown in Fig. 1(a)], and is measured to be approximately 16 mW. The power measured is that of the laser beam emitted from the objective. This power can be seen as the power of the light that reaches the substrate of the dielectric multilayer [glass, Fig. 1(b)]. It can be seen as the incident power. This incident power does not change when we change the incidence angle or incident polarization.

The illumination region of the laser beam is illustrated by the red dashed circles drawn in Figs. 2(a)–2(d). When the incident beam is TE polarized, we find a large-scale migration of colloidal particles radially toward the center of the illumination region, and aggregation into hexagonal close-packed colloidal crystals. The number of particles in Fig. 2(a) is much less than that in Fig. 2(d), meaning that particles with locations beyond the illumination

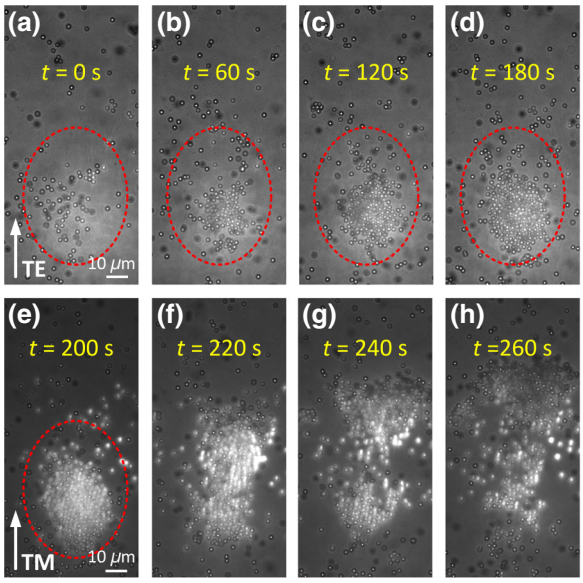

FIG. 2. Assembly and guidance of colloidal particles for an incidence angle of about 63°. (a)–(d) The incident laser beam is TE polarized. The colloidal particles are organized into hexagonal close-packed colloidal crystals during illumination. (e)–(h) The incident beam is changed to a TM-polarized beam; the packed colloidal particles are then guided along the propagation direction of the evanescent waves. The scale bar in (a) is also applicable to (b)–(h). The arrows in (a),(e) show the propagation direction of the evanescent waves in each case. The incident laser-beam power is approximately 16 mW. The dashed circles indicate the illumination region of the laser beam.

region or even the field of view (FoV) of the objective are also dragged into the illumination region. Once the incident polarization is changed to TM, the particles continue to migrate toward the illumination region at first, but after they enter the illumination region, these colloidal particles are rapidly guided along the propagation direction of the excited evanescent waves and stop around the edge of the illumination region as shown in Figs. 2(e)–2(h). Clearer demonstrations of the assembly and guidance of the colloidal particles using the two types of polarization can be found in Video 1 [38]. These phenomena demonstrate directly that in a 1DPC containing a PBG, the evanescent waves produced by a TE-polarized beam have a totally different effect on the colloidal particles from that produced by a TM-polarized beam, which has not previously been observed in the case of evanescent waves on a water-glass interface [36].

To qualitatively demonstrate the guidance of the particles [it happens only inside the laser illumination region, and means the movement of the particles along the propagation direction of the laser beam in the X-Y plane, shown by the arrows in Figs. 3(a) and 3(e)], we prepare dilute samples and measure the guidance velocity of individual colloidal particles inside the laser illumination region. As shown in Figs. 3(a)–3(h), the incidence angle is set to about 62°, where both the TM- and the TE-polarized laser beam can guide the particles in the laser illumination region, but with different average velocities (5.37 μm/s for the TM-polarized and 2.23 μm/s for the TE-polarized beam). The guidance velocity at other incidence angles is also measured, as shown in Fig. 3(i). For each incidence angle, the velocities of three individual particles are measured and then averaged to get the final velocity at this angle. The experimental results clearly demonstrate that the guidance velocity in the case of the TM-polarized beam is larger than that for the TE-polarized beam. For each of the two polarizations of the beam, when the incidence angle is increased, the guidance velocity reaches zero at some point (the particle is stable on the image), meaning that the individual particle is not guided along the propagation direction of the laser beam anymore.

When the incidence angle is increased further (such as to 65°), we find an assembly of particles outside and inside the laser illumination region for both the TM- and the TE-polarized laser beam. According to the BFP image [Fig. 1(c)] and the reflection curve [Fig. 1(d)], the internal mode appears in the 1DPC only for the TE-polarized beam with an incidence angle of about 65°. To test the changes in the manipulations of the colloidal particles that are possible, corresponding experiments at this incidence angle are carried out. The incident power is approximately 4 mW. Figures 4(a)–4(d) show that the colloidal particles are assembled quickly, even when the incident power is only one quarter of that used in the experiments shown in Figs. 2(a)–2(d). In contrast, at the same laser power (4 mW) and the same incidence angle, particles assemble very slowly for the TM polarization [Figs. 4(e)–4(h)]. Similarly, as in Figs. 2(a)–2(d), the number of particles in Fig. 4(a) [or Fig. 4(e)] is also much less than that in Fig. 4(d) [or Fig. 4(h)], so the particles beyond the FoV of

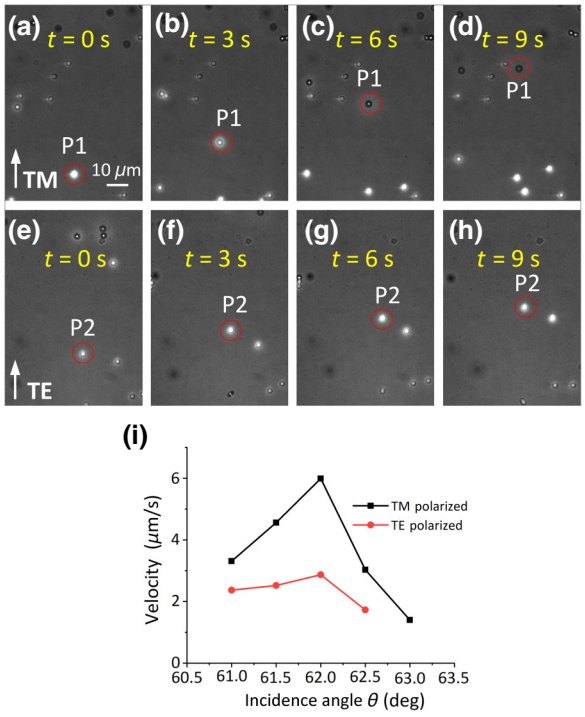

FIG. 3. Measuring the guidance velocity of a particle inside the laser illumination region. The incident power is 16 mW. (a)–(d) The incident beam is TM polarized. (e)–(h) The incident beam is TE polarized. The incidence angle is 62° (a)–(h). The positions of particles P1 and P2 on the image change with time, due to the guidance. (i) Guidance velocity vs incidence angle for TM- and TE-polarized illumination. The scale bar shown on (a) is also applicable to (b)–(h).

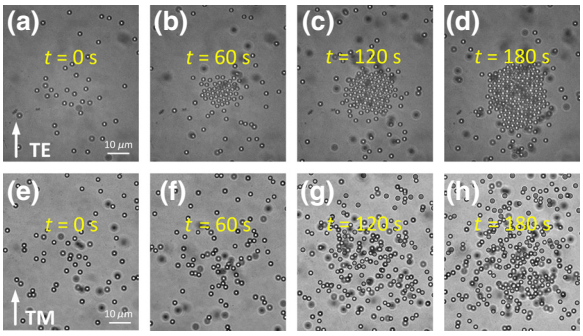

FIG. 4. Assembly of colloidal particles for an incidence angle of approximately 65°. The incident power is 4 mW. (a)–(d) The incident beam is TE polarized. (e)–(h) The incident beam is TM polarized. The scale bar shown on (a) is also applicable to (b)–(h).

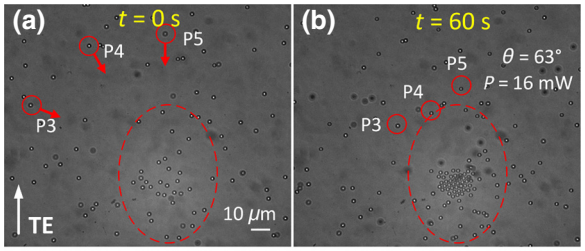

(c)

		TE polarized	TM polarized
63°	P = 16 mW	0.607 μm/s	0.677 μm/s
65°	P = 4 mW	0.738 μm/s	0.122 μm/s
	P = 16 mW	5.508 μm/s	1.081 μm/s

FIG. 5. Measuring the assembly velocity of particles outside the laser illumination region. This assembly is due to the thermal convection force. (a) At the moment $t = 0$ s, three individual particles (P3, P4, and P5) are outside and far away from the laser illumination region (marked by the red ring). (b) After laser illumination for 60 s, the three particles reach the boundary of the laser illumination region. The incident beam is TE polarized, the incident power is 16 mW, and the incidence angle is 63°. The scale bar shown on (a) is also applicable to (b). (c) Averaged assembly velocity of particles for various incident powers, incident polarizations, and incidence angles.

the microscope are also attracted to the laser illumination region.

As shown in Video 1 [38] and Figs. 2 and 4, the particles outside the laser illumination region are attracted to or assembled in the center, under both TM- and TE-polarized illumination and for different incidence angles. The average assembly velocity also can be measured from two images such as those shown in Figs. 5(a) and 5(b), which were recorded at $t = 0$ and $t = 60$ s, respectively. Here, the assembly velocities of three individual particles (P3, P4, and P5) are calculated and then an average velocity is obtained as shown in Fig. 5(c). It should be noted that this assembly velocity means the drag speed of the particles from outside the laser illumination region [Fig. 5(a)] to the boundary of the illumination region [Fig. 5(b)]. The assembly velocities for different incidence angles (63° and 65°), incident powers (4 and 16 mW), and polarizations (TE and TM) are all measured, as summarized in Fig. 5(c). It is clearly shown that the drag speed is largest when the internal mode is excited (TE polarized, $P = 16$ mW, and incidence angle 65°).

C. Numerical simulations of the photonic force and thermal convection

To derive the mechanisms of particle assembly and guidance as shown in Figs. 2–5, numerical simulations are performed as follows. In our experiments, the angle of incidence is larger than the critical angle, and evanescent waves are generated on the surface of the 1DPC. These evanescent waves induce scattering forces on the colloidal particles along the propagation direction of the waves, and a gradient force that points toward the multilayer. Three-dimensional finite-difference time-domain simulations [39, 40] are performed to calculate the angle-dependent scattering optical force (F_{SX}) and photonic gradient force (F_{GZ}), as shown in Figs. 6(a) and 6(b). In the simulations, the dielectric multilayers consist of alternating layers of SiO_2 (low refractive index, $n = 1.474 + i*10^{-4}$) and Si_3N_4 (high refractive index, $n = 2.498 + i*10^{-3}$), and the wavelength is 640 nm. The refractive indices of the water and the glass substrate are 1.33 and 1.515, respectively. The refractive index of the colloidal particles is 1.59. The incident power is set at 16 mW.

Figure 6(a) clearly demonstrates that the photonic scattering forces produced by the TM-polarized beam are stronger than those produced by the TE-polarized beam. The scattering forces decrease with increasing incidence angle (from 62° to 67°, larger than the critical angle). Figure 6(b) also demonstrates that the photonic gradient force drags the particles to the dielectric multilayer (the force is negative) when the incidence angle is larger than the TIR angle (62°) [36]. It also demonstrates that the photonic gradient force produced by the TM-polarized beam is larger than that produced by the TE-polarized beam. These numerical results can be explained through the electric-field distributions of the evanescent waves in Figs. 6(c)–6(f). The intensity of the evanescent waves at the 1DPC-water interface in the case of the TM-polarized incident beam [Figs. 6(d) and 6(f)] is stronger than that for the TE-polarized incident beam [Figs. 6(c) and 6(e)] when the incidence angles of the two polarized beams are the same. The stronger the electromagnetic field at the water-1DPC interface, the larger the scattering force enabled by this optical field. Similarly, for the TM-polarized incident beam, with increasing incidence angle, the intensity of the evanescent waves at the 1DPC-water interface decreases, and then the scattering force weakens, such as in Fig. 6(d) compared with Fig. 6(f).

The scattering force enabled by the evanescent waves can be used to explain the guidance of colloidal particles inside the laser illumination region as shown in Figs. 2(e)–2(h) and 3, where the strong scattering force produced by the TM-polarized beam can guide the motion of the particles along the propagation direction of the evanescent waves. This guidance does not happen when the polarization is switched to TE [Figs. 2(a)–2(d)] or when the incidence angle is increased (Fig. 4), when the scattering force enabled by the propagating evanescent waves is greatly decreased to nearly zero, as shown in Fig. 6(a). Another piece of evidence that the guidance is due to the optical scattering force is that this guidance stops when the particles are outside the laser illumination region (as clearly shown in Video 1 [38]), where there is no electric field.

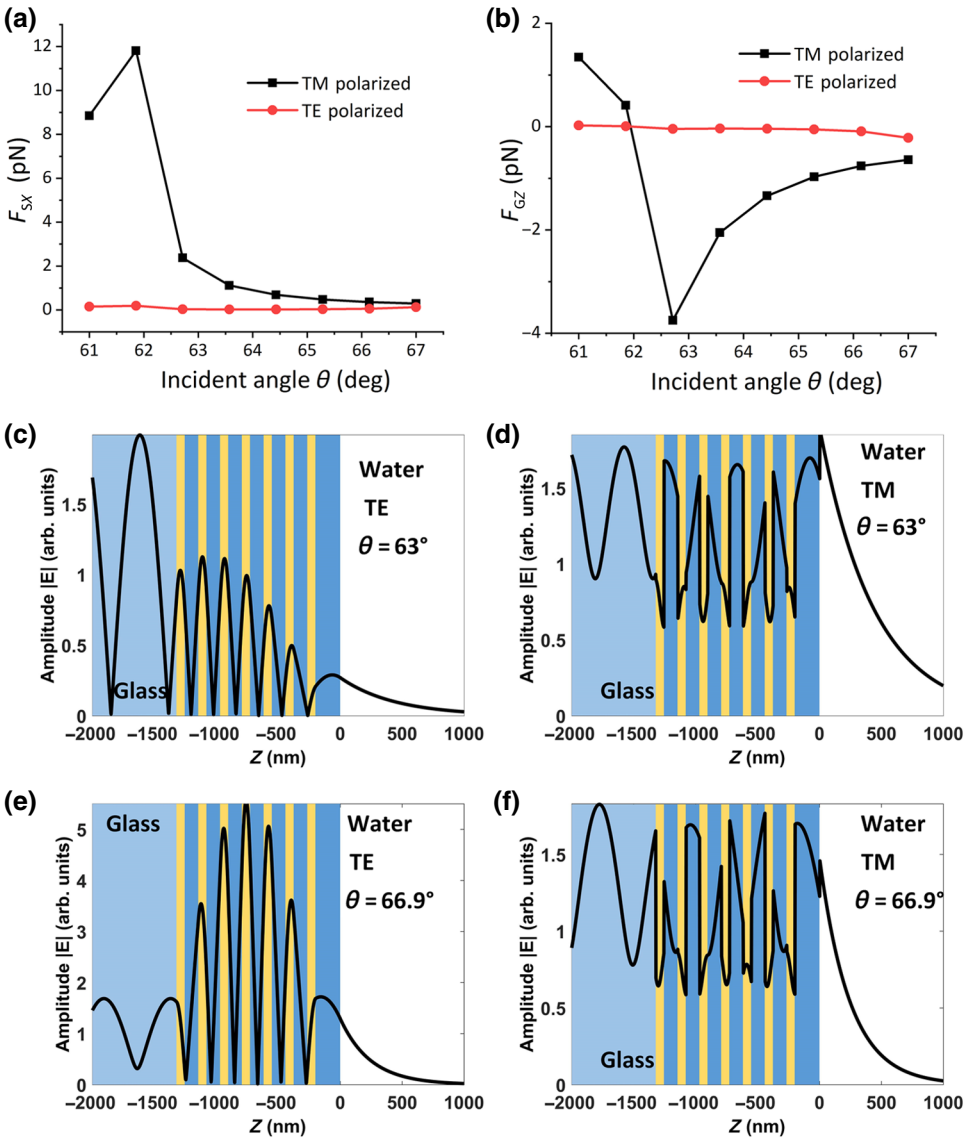

FIG. 6. Numerical simulations of the optical-force and electric-field distributions. (a),(b) Calculated optical scattering force (F_{SX}) and optical gradient force (F_{GZ}) as a function of the incidence angle. (c),(d) Electric-field distributions under TE- (c) and TM-polarized (d) illumination, when the angle of incidence is fixed at 63°. (e),(f) The same distributions when the angle of incidence is fixed at 66.9°, corresponding to the excitation angle for the internal mode, as shown in Fig. 1(d). The position $Z = 0$ nm denotes the water-1DPC interface.

On the contrary, for the assembly of particles, as demonstrated in Sec. IIB (Figs. 2(a)–2(d), 4, and 5, and Video 1 [38]), even particles beyond the laser illumination region, where there are no electromagnetic fields, can be assembled. So, the assembly of particles is due to a long-range interaction and cannot be attributed to the optical scattering or gradient force. When we turn to the electric-field distributions in Figs. 6(c), 6(e), and 6(f), we find that the electric field inside the multilayer is stronger than that at the 1DPC-water interface. Because of the intrinsic loss of the dielectric multilayer, heat is unavoidably generated under continuous illumination with the laser beam [Fig. 1(b)] and results in a temperature gradient in the 1DPC. We deduce that the mechanism of the assembly of particles is due to a temperature-gradient-induced convective flow of the water solution, which is consistent with the phenomenon of long-range capture of microparticles around the center of a beam by the generation of local heat [24,41].

In order to verify this judgment, COMSOL Multiphysics Ver. 5.4 [42] is used to conduct an analysis of thermal convective flow with the same optical configuration as that shown in Fig. 1(b). For simplification, the velocity of the water flow is simulated based on two-dimensional (2D) heat conduction, the thickness of the water film is set to 100 μm, and the initial temperature of the system is set to 293.15 K. All other structural parameters are the same as those shown in Fig. 1(b).

Figure 7 shows the simulation results, where the arrows indicate the flow direction of the water and can also represent the direction of the convective force on the particles. From the flow directions in Fig. 7, we can judge that the colloidal particles are attracted to the center of the illumination region ($X = 0$ μm), which is attributed to the

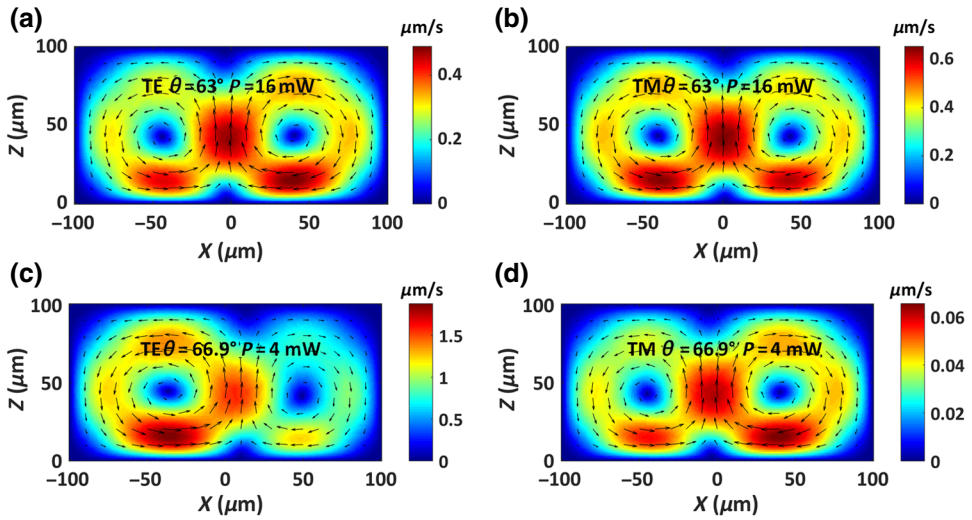

FIG. 7. Maps of simulated 2D convective velocity around the beam center ($X = 0$ μm). The arrows indicate the directions of water flow, and the scale bars (on the right side of each image) express the magnitude of the velocity. (a)–(d) Calculated fluid convection pattern for different polarizations (TE, TM), incidence angles (θ), and incident powers (P). (a) TE polarized, $\theta = 63°$, $P = 16$ mW; (b) TM polarized, $\theta = 63°$, $P = 16$ mW; (c) TE polarized, $\theta = 66.9°$, $P = 4$ mW; (d) TM polarized, $\theta = 66.9°$, $P = 4$ mW.

temperature-gradient-induced convective flow of the water solution. The scale bars (on the right-hand side of each image) in Fig. 7 represent the flow velocity, and can also represent the magnitude of the convective forces enabled on the colloidal particles.

When comparing Figs. 7(a) and 7(b) (corresponding to the experimental results shown in Fig. 2, where the incidence angle is 63°), we see that the convective forces induced by the temperature gradient under illumination with the TE- and TM-polarized laser beams are nearly the same, and hence the colloidal particles would be assembled in both of these two cases, which is consistent with the experimental results shown in Fig. 5, where the colloidal particles outside the laser illumination region are assembled and attracted to the laser illumination region at nearly the same assembly velocity (the incidence angle is 63° and the incident power is 16 mW, for both TM- and TE-polarized illumination). When these particles are attracted into the laser illumination region, as shown in Fig. 2, the TM-polarized illumination guides the particles along the propagation direction of the laser beam in the X-Y plane [Figs. 2(e)–2(h) and Video 1 [38]]; however, the TE-polarized beam attracts the particles further to the center and increases the amount of assembly [Figs. 2(a)–2(d) and Video 1 [38]]. This difference inside the laser illumination region can be explained by the calculated optical scattering force as shown in Fig. 6(a). When the incidence angle is 63°, the optical scattering force is much stronger for TM-polarized illumination, which suppresses the convective force and then induces guidance of the particles along the propagation direction of the evanescent waves [Figs. 2(e)–2(h) and 3]. In contrast, in the case of TE-polarized illumination, the scattering force is near zero, and then the convective force is dominant and results in assembly as shown in Figs. 2(a)–2(d).

When the incidence angle is increased, such as to 67°, due to the greater confinement of the electric field inside the 1DPC [especially for the internal mode excited by the TE-polarized beam, Fig. 6(e)], more heat is generated and then results in a larger convective force [as shown in the scale bar in Fig. 7(c)]. The incident power is only 4 mW, but the flow velocity in Fig. 7(c) is still larger than that in Fig. 7(a) (where the power is 16 mW). At this incidence angle, the optical scattering force is nearly zero for both polarizations [Fig. 6(a)], and so the convective forces are dominant, which results in the assembly of the colloidal particles as shown in Figs. 4(a)–4(d).

When comparing Figs. 7(c) and 7(d), we find that the flow velocity in the case of TM-polarized illumination is much smaller than that for TE-polarized illumination, which can be attributed to the electric-field distribution inside the 1DPC [Figs. 6(e) and 6(f)]. The smaller flow velocity results in a smaller convective force, and the assembly speed of the colloidal particles is much smaller, which is consistent with the experimental results shown in Figs. 4(e)–4(h) and 5(c) [the assembly velocity in the case of the TM-polarized beam (0.122 μm/s) is much smaller than that for the TE-polarized beam (0.738 μm/s) for an incidence angle of 65° and a power of 4 mW].

From the simulated flow directions as shown in Fig. 7, we notice that an assembled particle (around the position $X = 0$ μm) can be pushed upward and away from the water-1DPC interface if the convective force is larger than the gravity force on the particle. This is verified by our experimental results, as shown in Fig. 8. A TE-polarized beam is used to excite the internal mode of the 1DPC. When the incident power is increased, more heat is generated inside the multilayer structure, resulting in a stronger convective force. When the incident power is only 5 mW, the colloidal particles are organized into close-packed hexagonal colloidal crystals [see Figs. 8(a) and 8(b)]. As the incident power increases, reaching up to 12 mW, the number of organized particles in the illuminated region (marked using a dashed circle) decreases under continuous

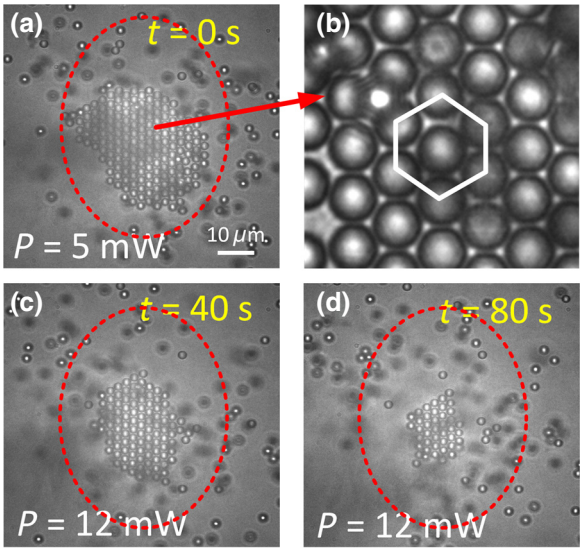

FIG. 8. Effect of incident power on assembly of colloidal particles. The internal mode of the 1DPC is excited by a TE-polarized laser beam. The incident power is increased from 5 mW (a) to 12 mW (c), (d). (b) Enlarged image of the assembled particles showing a hexagonal pattern. The scale bar on (a) is also applicable to (c),(d).

illumination, as shown in Figs. 8(c) and 8(d). A clearer demonstration of the escape of these organized particles from the illuminated region is presented in Video 2 [43], showing that the particles are pushed upward due to the convective force being larger than the gravity force on the particles.

III. CONCLUSIONS

In summary, we demonstrate that evanescent waves on an all-dielectric 1DPC allow the use of combined optical and thermal forces for either guiding or assembling colloidal particles, simply by tuning the polarization and angle of the incident laser beam. This can be used to create an optical conveyor belt for the sampling and sorting of large-scale assemblies of micro-objects, which indicates an alternative potential use for 1DPCs. These phenomena are not observed for evanescent waves excited on a conventional water-glass interface. The mechanism of this guidance and assembly is analyzed based on competition between the optical scattering force and the optically induced thermal convective force. When the optical scattering force is larger, the particles are guided along the direction of the propagating evanescent waves inside the laser illumination region, such as when TM-polarized incidence was used and the incidence angle was 63°. In contrast, when the convective force is larger, such as when a TE-polarized laser beam with an incidence angle larger than the TIR angle is used, the colloidal particles are assembled from outside the laser illumination region to the inside. If the convective force is increased further by using a high laser power, the assembled particles can be pushed away from the 1DPC substrate, because the convective force becomes larger than the gravity force on the particles.

It should be noted here that while our experiments are performed with a high-NA objective, they can also be done using a setup based on a high-refractive-index prism, where more colloidal particles can be accumulated in the excitation region; in addition, the motion areas of these particles can be larger because the excitation region on the prism is larger than that on an objective lens [41,44]. However, the advantage of the objective-based experimental setup is also obvious; its imaging ability can be used to monitor the manipulation of the particles directly while also capturing surface-enhanced Raman spectra, and it can also be used to study light-induced self-assembly and optical binding interactions, along with the nonlinear properties of densely packed metal or dielectric particle arrays. We describe an optical-microscope system that is capable of both guiding and trapping dielectric particles using only one laser beam. This method can be used for applications including the accumulation, microfiltration, and transportation of microscale or submicroscale particles or biological materials. The attraction of many particles into the illumination region when thermal convection is created might find applications in research on prebiotic evolution. One of the main requirements in prebiotic studies of self-replicating systems and of prebiotic metabolisms [24] is high concentrations of reaction partners. It appears likely that the thermal convection force can cause reaction partners (similar to the colloidal particles used in our experiment) to be drawn to the center of the excited region, and then their concentrations can be greatly increased. The ability to generate local heat inside the 1DPC substrate can also be used to develop thermophoretic tweezers that can be used to manipulate colloidal particles, living cells, and other bodies [45–47].

ACKNOWLEDGMENTS

This work was supported by the National Nature Science Foundation of China (Grants No. 61427818 and No. 11774330), the Ministry of Science and Technology of China (Grant No. 2016YFA0200601), the Anhui Initiative in Quantum Information Technologies, the Science and Technological Fund of Anhui Province for Outstanding Youth (Grant No. 1608085J02), Anhui Provincial Science and Technology Major Projects (Grant No. 18030901005), the Fundamental Research Funds for the Central Universities (Grant No. WK2340000084), the foundation of the Key Laboratory of Environmental Optics and Technology of the Chinese Academy of Sciences (Grant No. 2005DP173065-2019-XX), and the Longshan Academic Talent Research Supporting Program of SWUST (Grant No. 17LZX626). D.G.Z is also supported by a USTC

Tang Scholarship. JRL acknowledges support from grants from the National Institute of Health (Grants No. R01 GM125976 and No. R21 GM129561). The work was partially carried out at the University of Science and Technology of China's Center for Micro and Nanoscale Research and Fabrication.

[1] A. Ashkin, Optical trapping and manipulation of neutral particles using lasers, Proc. Natl. Acad. Sci. U.S.A. **94**, 4853 (1997).
[2] A. N. Grigorenko, N. W. Roberts, M. R. Dickinson, and Y. Zhang, Nanometric optical tweezers based on nanostructured substrates, Nat. Photonics **2**, 365 (2008).
[3] K. C. Neuman and S. M. Block, Optical trapping, Rev. Sci. Instrum. **75**, 2787 (2004).
[4] P. M. Hansen, V. K. Bhatia, N. Harrit, and L. Oddershede, Expanding the optical trapping range of gold nanoparticles, Nano Lett. **5**, 1937 (2005).
[5] A. Lehmuskero, P. Johansson, H. Rubinsztein-Dunlop, L. M. Tong, and M. Kall, Laser trapping of colloidal metal nanoparticles, ACS Nano **9**, 3453 (2015).
[6] A. Ashkin, J. M. Dziedzic, and T. Yamane, Optical trapping and manipulation of single cells using infrared-laser beams, Nature **330**, 769 (1987).
[7] A. Ashkin, J. M. Dziedzic, J. E. Bjorkholm, and S. Chu, Observation of a single-beam gradient force optical trap for dielectric particles, Opt. Lett. **11**, 288 (1986).
[8] V. Garces-Chavez, K. Dholakia, and G. C. Spalding, Extended-area optically induced organization of microparticles on a surface, Appl. Phys. Lett. **86**, 031106 (2005).
[9] J. R. Arias-Gonzalez and M. Nieto-Vesperinas, Optical forces on small particles: Attractive and repulsive nature and plasmon-resonance conditions, J. Opt. Soc. Am. A **20**, 1201 (2003).
[10] D. Erickson, X. Serey, Y. F. Chen, and S. Mandal, Nanomanipulation using near field photonics, Lab Chip **11**, 995 (2011).
[11] M. L. Juan, M. Righini, and R. Quidant, Plasmon nano-optical tweezers, Nat. Photonics **5**, 349 (2011).
[12] K. Wada, K. Sasaki, and H. Masuhara, Optical measurement of interaction potentials between a single microparticle and an evanescent field, Appl. Phys. Lett. **76**, 2815 (2000).
[13] G. Volpe, R. Quidant, G. Badenes, and D. Petrov, Surface Plasmon Radiation Forces, Phys. Rev. Lett. **96**, 238101 (2006).
[14] B. S. Schmidt, A. H. J. Yang, D. Erickson, and M. Lipson, Optofluidic trapping and transport on solid core waveguides within a microfluidic device, Opt. Express **15**, 14322 (2007).
[15] M. Righini, G. Volpe, C. Girard, D. Petrov, and R. Quidant, Surface Plasmon Optical Tweezers: Tunable Optical Manipulation in the Femtonewton Range, Phys. Rev. Lett. **100**, 186804 (2008).
[16] K. Wang, E. Schonbrun, P. Steinvurzel, and K. B. Crozier, Scannable plasmonic trapping using a gold stripe, Nano Lett. **10**, 3506 (2010).
[17] S. Duhr and D. Braun, Why molecules move along a temperature gradient, Proc. Natl. Acad. Sci. U.S.A. **103**, 19678 (2006).
[18] H. R. Jiang, H. Wada, N. Yoshinaga, and M. Sano, Manipulation of Colloids by a Nonequilibrium Depletion Force in a Temperature Gradient, Phys. Rev. Lett. **102**, 208301 (2009).
[19] E. Flores-Flores, S. A. Torres-Hurtado, R. Paez, U. Ruiz, G. Beltran-Perez, S. L. Neale, J. C. Ramirez-San-Juan, and R. Ramos-Garcia, Trapping and manipulation of microparticles using laser-induced convection currents and photophoresis, Biomed. Opt. Express **6**, 4079 (2015).
[20] R. Piazza and A. Guarino, Soret Effect in Interacting Micellar Solutions, Phys. Rev. Lett. **88**, 208302 (2002).
[21] H. B. Xin and B. J. Li, Targeted delivery and controllable release of nanoparticles using a defect-decorated optical nanofiber, Opt. Express **19**, 13285 (2011).
[22] M. Righini, C. Girard, and R. Quidant, Light-induced manipulation with surface plasmons, J. Opt. A: Pure Appl. Opt. **10**, 093001 (2008).
[23] J. Chikazawa, T. Uwada, A. Furube, and S. Hashimoto, Flow-induced transport via optical heating of a single gold nanoparticle, J. Phys. Chem. C **123**, 4512 (2019).
[24] D. Braun and A. Libchaber, Trapping of DNA by Thermophoretic Depletion and Convection, Phys. Rev. Lett. **89**, 188103 (2002).
[25] P. Yeh, A. Yariv, and C. S. Hong, Electromagnetic propagation in periodic stratified media. 1. General theory, J. Opt. Soc. Am. **67**, 423 (1977).
[26] Y. Augenstein, A. Vetter, B. V. Lahijani, H. P. Herzig, C. Rockstuhl, and M. S. Kim, Inverse photonic design of functional elements that focus Bloch surface waves, Light: Sci. Appl. **7**, 104 (2018).
[27] A. Angelini, A. Lamberti, S. Ricciardi, F. Frascella, P. Munzert, N. De Leo, and E. Descrovi, In-plane 2D focusing of surface waves by ultrathin refractive structures, Opt. Lett. **39**, 6391 (2014).
[28] I. V. Soboleva, V. V. Moskalenko, and A. A. Fedyanin, Giant Goos-Hanchen Effect and Fano Resonance at Photonic Crystal Surfaces, Phys. Rev. Lett. **108**, 123901 (2012).
[29] D. A. Shilkin, E. V. Lyubin, I. V. Soboleva, and A. A. Fedyanin, Direct measurements of forces induced by Bloch surface waves in a one-dimensional photonic crystal, Opt. Lett. **40**, 4883 (2015).
[30] F. Giorgis, E. Descrovi, C. Summonte, L. Dominici, and F. Michelotti, Experimental determination of the sensitivity of Bloch Surface Waves based sensors, Opt. Express **18**, 8087 (2010).
[31] E. Descrovi, T. Sfez, M. Quaglio, D. Brunazzo, L. Dominici, F. Michelotti, H. P. Herzig, O. J. F. Martin, and F. Giorgis, Guided Bloch surface waves on ultrathin polymeric ridges, Nano Lett. **10**, 2087 (2010).
[32] Y. Kuai, J. X. Chen, X. Tang, Y. F. Xiang, F. Y. Lu, C. F. Kuang, L. Xu, W. D. Shen, J. J. Cheng, H. Q. Gui, G. Zou, P. Wang, H. Ming, J. G. Liu, X. Liu, J. R. Lakowicz, and D. G. Zhang, Label-free surface-sensitive photonic microscopy with high spatial resolution using azimuthal rotation illumination, Sci. Adv. **5**, eaav5335 (2019).

[33] J. D. Joannopoulos, Photonic crystals molding the flow of light, J. Occup. Med. Toxicol. **375**, 278 (1995).
[34] J. X. Chen, D. G. Zhang, P. Wang, H. Ming, and J. R. Lakowicz, Strong Polarization Transformation of Bloch Surface Waves, Phys. Rev. Appl. **9**, 024008 (2018).
[35] D. G. Zhang, R. Badugu, Y. K. Chen, S. S. Yu, P. J. Yao, P. Wang, H. Ming, and J. R. Lakowicz, Back focal plane imaging of directional emission from dye molecules coupled to one-dimensional photonic crystals, Nanotechnology **25**, 145202 (2014).
[36] S. Kawata and T. Sugiura, Movement of micrometer-sized particles in the evanescent field of a laser-beam, Opt. Lett. **17**, 772 (1992).
[37] E. Anemogiannis, E. N. Glytsis, and T. K. Gaylord, Determination of guided and leaky modes in lossless and lossy planar multilayer optical waveguides: Reflection pole method and wavevector density method, J. Lightwave Technol. **17**, 929 (1999).
[38] See the Supplemental Material at http://link.aps.org/supplemental/10.1103/PhysRevApplied.13.014020 for [Assembly of the colloidal particles using the TE-polarized beam and guiding the particles using the TM-polarized beam when the angle of incidence was set at 63°. The red ring indicates the position of the laser illumination region].
[39] A. Taflove, and S. C. Hagness, Computational electrodynamics: The finite-difference time-domain method, 3rd edition, J. Comput. Methods Sci. Eng. (Artech House Publishers, 2005).
[40] P. H. Jones, O. M. Maragò, and G. Volpe, *Optical Tweezers: Principles and Applications* (Cambridge University Press, London, 2015).
[41] V. Garces-Chavez, R. Quidant, P. J. Reece, G. Badenes, L. Torner, and K. Dholakia, Extended organization of colloidal microparticles by surface plasmon polariton excitation, Phys. Rev. B **73**, 085417 (2006).
[42] http://www.comsol.com.
[43] See the Supplemental Material at http://link.aps.org/supplemental/10.1103/PhysRevApplied.13.014020 for [Escape of the organized particles from the illuminated region when the incident power increased. The internal mode was excited using the TE-polarized beam. The red ring indicates the position of the laser illumination region].
[44] M. Siler, T. Cizmar, A. Jonas, and P. Zemanek, Surface delivery of a single nanoparticle under moving evanescent standing-wave illumination, New J. Phys. **10**, 113010 (2008).
[45] L. Lin, M. S. Wang, X. L. Peng, E. N. Lissek, Z. M. Mao, L. Scarabelli, E. Adkins, S. Coskun, H. E. Unalan, B. A. Korgel, L. M. Liz-Marzan, E. L. Florin, and Y. B. Zheng, Opto-thermoelectric nanotweezers, Nat. Photonics **12**, 195 (2018).
[46] L. H. Lin, X. L. Peng, X. L. Wei, Z. M. Mao, C. Xie, and Y. B. Zheng, Thermophoretic tweezers for Low-power and versatile manipulation of biological cells, ACS Nano **11**, 3147 (2017).
[47] L. H. Lin, E. H. Hill, X. L. Peng, and Y. B. Zheng, Optothermal manipulations of colloidal particles and living cells, Acc. Chem. Res. **51**, 1465 (2018).